PENNSTATE

Applied Research Laboratory

TRANSLATION OF AIRFOIL TRAILING EDGE NOISE ARTICLE FROM *REVUE D'ACOUSTIQUE*

R. C. Marboe and R. M. Weyer

Technical Memorandum
File No. 91-120
25 June 1991

Copy No. 14

Applied Research Laboratory
P.O. Box 30
State College, PA 16804
(814) 865-3031

Contracted by the Department of the Navy
Space and Naval Warfare Systems Command
Contract No. N00039-88-C-0051

TRANSLATION OF AIRFOIL TRAILING EDGE NOISE ARTICLE FROM *REVUE D'ACOUSTIQUE*

R. C. MARBOE AND R. M. WEYER

Technical Memorandum
File No. 91-120
25 June 1991

Abstract: The paper "Bruit d'un profil dans un écoulement", by P. Garcia and P. Gerard, has been translated into English. The paper originally was published in *Revue d'Acoustique*, No. 73, 1985 2/4 by Office National d'Etudes et de Recherches Aerospatiales (ONERA). The work, "Airfoil noise in air flow", describes measurements of the wave number spectrum of the turbulent boundary layer induced pressure field in the vicinity of the airfoil trailing edge. An estimate of radiated noise using modifications to the theories of Howe and Hogdson is made. The paper is significant because of the good agreement between the measurements of Brooks and Hogdson (1980) and a predicted radiated noise level based on a measured trailing edge fluctuating pressure wave number spectrum with measured far field radiated noise. An effect of array element separation distance on measured convection velocity is also shown.

Acknowledgement: This translation was performed in support of ARL vehicle radiated noise model development.

The authors wish to thank L. Kovarovic, instructor in the French Department at The Pennsylvania State University, for her review.

ORIGINALLY ISSUED AS AN IM 2 MAY 1991

The contractor, The Pennsylvania State University, hereby certifies that, to the best of its knowledge and belief, the technical data delivered herewith under Contract No. N00039-88-C-0051 is complete, accurate, and complies with all requirements of the contract.

Date: 25 June 1991

Name and Title of Certifying Official: L. R. Hettche

Dr. L. R. Hettche, Project Director

Translated by R. C. Marboe and R. M. Weyer, 19 April 1991

Airfoil Noise in Air Flow

by P. Garcia and P. Gerard

Revue d'Acoustique, No. 73, 1985, 2/4
Office National d'Etudes et de Recherches Aerospatiales (ONERA)

Manuscript received 14 November 1984, revised 5 February 1985.

ABSTRACT

An experimental investigation of the NACA 0012 airfoil noise in a uniform flow has been conducted in the anechoic open flow facility CEPRA 19.

The purpose of these studies is an estimation of the radiated noise deduced from theoretical models developed by Howe and Hogdson. These models need the spectral characteristics of the turbulent boundary layer induced pressure field in the vicinity of the trailing edge.

The airfoil has been instrumented by longitudinal and transverse arrays of surface pressure sensors allowing the determination of the wavenumber spectrum of the turbulent boundary layer. These measurements are used as the input data for a prediction method.

CONVENTIONS AND NOTATIONS

$A(\omega\epsilon_1/\bar{V})$, $B(\omega\epsilon_3/\bar{V})$	Corcos functions [5]
c	Speed of sound
f	Frequency
G_{uv}	Cross-spectrum between the signals u and v
G_{uu}, G_{vv}	Autospectra of signals u and v
k	Wave number defined by 2π f/V
$\bar{k}$	Wave number defined by f/V

ℓ_1, ℓ_3	Longitudinal and transverse turbulence integral scales
L	Airfoil span (1.60 m) interacting with a uniform flow
L_H	Airfoil span of Brooks and Hogdson [11] (40 cm)
$p(x_1,x_3,t)$	Time dependent pressure at point (x_1,x_3)
$P(k_1,k_3,\omega)$	Space-time Fourier transform of $p(x_1,x_3,t)$
R	Distance between the source and the receiver (1.80 m)
R_H	Distance between the source and the receiver for Brooks and Hogdson (1.20 m)
R_e	Reynolds number
R_{ef}	Effective transducer radius
$S(\omega)$, $S(f)$	Acoustic power spectral density
t	Time
U_o	Freestream velocity
$\overline{V} = 0.8\ U_o$	Mean convection velocity
x_1, x_3	Longitudinal and transverse coordinates on the surface of the airfoil
γ	Coherence function
δ^*	Displacement thickness of the turbulent boundary layer
η_1, η_3	Longitudinal and transverse exponential decay factors
Θ	Observation angle in the horizontal plane ($\Theta = 0$ corresponds to the downstream direction)
$\Phi_{TBL}(k_1,k_3,\omega)$	Wave number spectrum of the induced fluctuating pressure under the turbulent boundary layer
$\Phi_{TE}(k_1,k_3,\omega)$	Wave number spectrum of the induced fluctuating pressure in the proximity of the trailing edge
$\Phi_1(k_1)$, $\Phi_3(k_3)$	Longitudinal and transverse wave number spectra
$\Phi(\omega)$	Fluctuating pressure spectral density
ϵ_1, ϵ_3	Longitudinal and transverse separations between two transducers

Δx_1, Δx_3 Longitudinal and transverse separations between pressure transducers that form the array
Longitudinal array, short Δx_1 = 6 mm, medium Δx_1 = 18 mm
Transverse array, short Δx_3 = 3 mm, long Δx_3 = 12 mm

ρ Density

τ_{opt} Delay due to convection, corresponding to the maximum of the cross-correlation

1. INTRODUCTION

The preliminary results presented in this article are relative to the trailing edge noise of a NACA 0012 airfoil in a uniform flow, at low Mach number (M=0.2) and at Reynolds number, Re = 2 x 10^6, calculated based upon a chord of 50 cm. The tests took place in the open jet anechoic wind tunnel, CEPRA 19.

The models developed by Ffowcs Williams and Hall [1], among others, through the acoustic analogy of Lighthill; by Chase [2] and Chandiramani [3] for hydroacoustic techniques and, more recently by Howe [4] aided by a unified theory, attempt to estimate the noise radiated by a half-plane in a uniform flow. Howe has shown, in particular, that for low Mach numbers these theories lead to similar results.

In this article, the estimation of radiated noise by a NACA 0012 airfoil will be made using a simplified formulation, given by Howe [4]. Its usage requires knowledge, in the proximity of the trailing edge, of the wall pressure spectral densities induced by a turbulent boundary layer $\Phi(\omega)$, as well as the transverse integral scales of turbulence, ℓ_3.

These characteristics of the turbulence are obtained from experimental results for a fully developed turbulent boundary layer in the following conditions: an airfoil with tripped transition, an incidence angle of 0.4°, and a velocity of 60 m/s.

The experimental model and instrumentation set-up placed in CEPRA 19 is presented in the first part. Then experimental results relative to the fluctuating pressure field are given in the form of spectral densities, according to the model of Corcos [5], and wave number spectra.

Finally, the noise radiated by an airfoil is identified and localized due to the technique of acoustical imagery and measured cross-spectra, then compared to the results of the simplified prediction calculations.

2. TEST CONDITIONS AND SIGNAL PROCESSING TECHNIQUES

2.1. Open Flow Facility CEPRA 19

The wind tunnel CEPRA 19 is an anechoic open jet wind tunnel. It has been configured with a removable nozzle 2.0 m in diameter. Under these conditions, the test jet occupies an approximately cylindrical volume of which the diameter and the length are 2.0 and 10.6 m respectively. The velocity of the flow is kept between 40 and 100 m/sec.

Figure 1 represents, schematically, the installation of the experimental device placed in the anechoic wind tunnel in order to conduct the tests. It includes, essentially, the NACA 0012 airfoil and an array of microphones situated vertically external to the flow (Figure 2).

2.2. NACA 0012 Model

2.2.1. Assembly

The airfoil is placed vertically in the wind tunnel. The trailing edge is situated about 2 m from the exit plane of the nozzle (Figures 1 and 2). A device permits adjustment of the angle of attack of the airfoil.

The results presented in this article have been obtained with an incidence angle near 0°, more exactly, 0.4°, with the trailing edge slightly directed toward the side wall of the wind tunnel (Figure 1).

The model, of which the span and chord are equal at 3.5 m, is made up of a stratified skin, reinforced by a metallic frame. A foam is injected between the frame and the skin in order to deaden vibrations. Strips of roughness, 2 cm wide, have been placed at 15% of the chord from the leading edge.

2.2.2. Instrumentation

It is in the form of an array of fluctuating pressure transducers, flush mounted, and of static pressure ports distributed along the chord on the lower face and the upper face.

2.2.2.1. Arrays (Figure 3)

The model is equipped with unsteady pressure sensors. These sensors are distributed in arrays: medium, short and long, and longitudinal and transverse arrays. This instrumentation is situated near the trailing edge. Two types of sensors are used:

* Entran EPIL 203A - They have a diameter of 2.03 mm and of a length of 5 mm, and are integrated in a small transverse bar of about 100 mm within 3 mm of the trailing edge. There are 15 of them. These sensors are placed near the trailing edge parallel to the surface of the airfoil, and connected to the latter by a cylindrical cavity of approximate length 2 mm and diameter 1 mm. A study of the amplitude and phase response of the transducer in the presence of this cavity has been made by CERT/ONERA [6]. The acoustical resonance frequency has been identified as 13 kHz. Accounting for the diameter of the cavity, the cutoff frequency of the device is estimated [7], for an attenuation of 5 dB

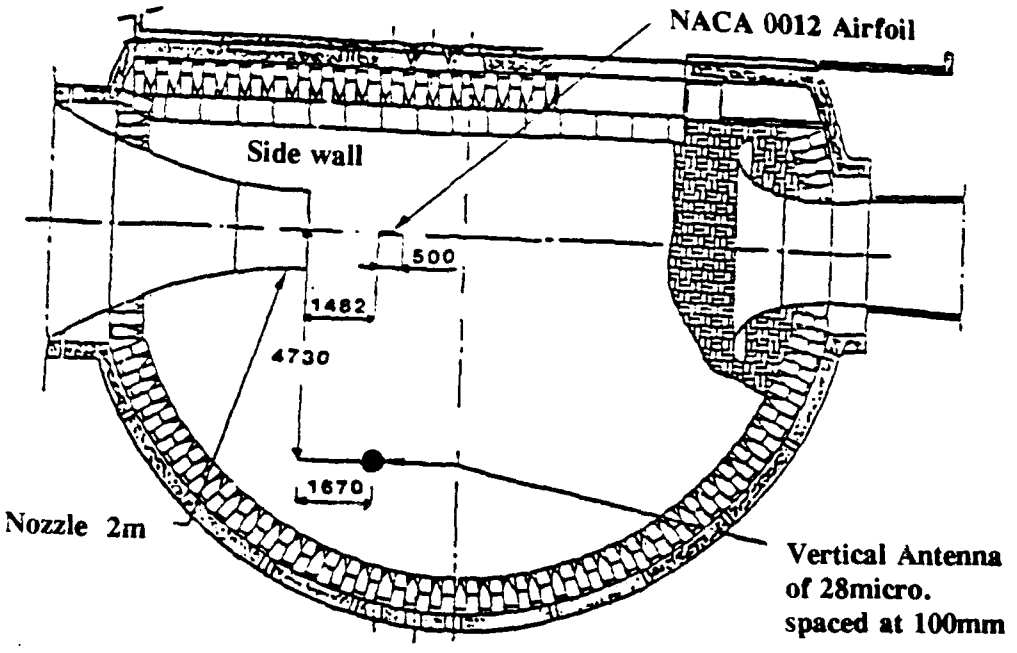

Figure 1. Experimental set-up of the model and the vertical antenna in CEPRA 19.

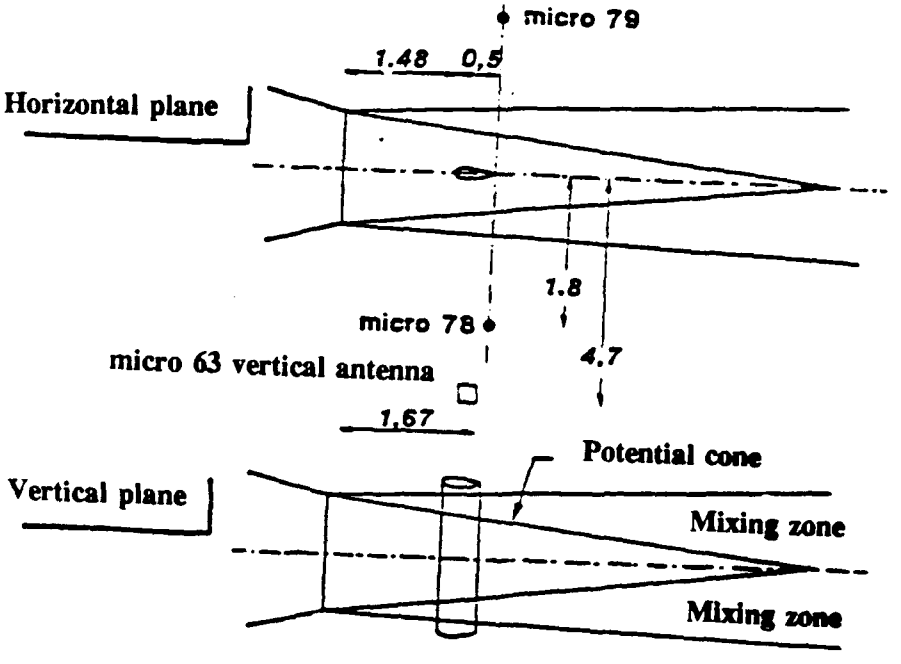

Figure 2. Experimental set-up of the NACA 0012 model and the instrumentation.

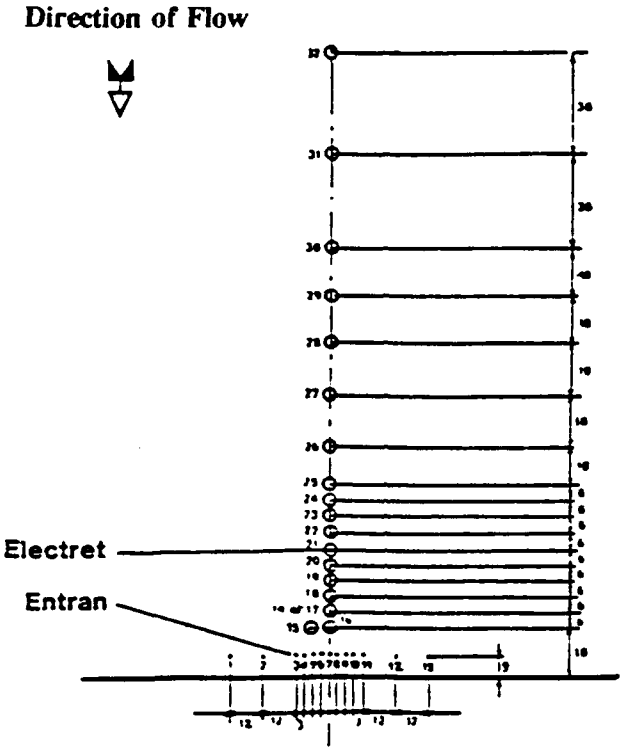

Figure 3. Trailing edge instrumentation.

of the wall pressure, approximately by:

$$f = \frac{0.8 \times 60}{2\pi \times 0.5 \times 10^{-3}} = 15 \text{ kHz}$$

* Electret sensors - These sensors are based on the "electret" effect, which is known as the quasi-permanent electrostatic polarization of a plastic membrane, of which the geometric radius is 1.8 mm. In these conditions of measuring wall pressure, its effective radius is about 1.08 mm (0.6 x 1.8) where the cutoff frequency is estimated to be 7 kHz. They are placed in line along the chord, perpendicular to the bar of Entran sensors.

2.2.2.2. Static Pressure Ports

A series of 47 local static pressure taps have been arranged along the chord on the lower and upper faces in order to measure the pressure distribution. These taps are linked by a pressure switch to 48 supply lines from a differential pressure transducer rated at ± 34.5 kPa. The pressure distribution along the chord allows the calculation of the incidence of the airfoil.

2.3. Instrumentation outside of the model

It is made up of a multimicrophone array (acoustic antenna) and of 2 B&K model 4135 microphones placed symmetrically. The multimicrophone array is composed of 28 B&K microphones spaced 10 cm apart, on a 2.7 m long beam placed outside of the flow and parallel to the trailing edge of the airfoil (Figure 2).

2.4. Acquisition and signal processing

For each test, the signals from the different transducers are amplified (research amplifiers that automatically set the gain, developed by ONERA) and are recorded on three 28 track tape recording devices. Parallel to these recording devices, a Fourier analyzer, model HP 5451 B dealt with, in real time, the signals of any three transducers allowing initial results to be acquired during the test. The set of results obtained in the Fourier system is stored numerically on magnetic tape in order to be played back on the CYBER system at ONERA. A complete package for analyzing the measurements and for graphical output has been developed at ONERA.

The multisensor computations are made with the aid of a vector processor AP 120 (Floating Point System), connected to an HP 1000 computer. In this way, one obtains an acoustic image of sources of noise. The adaptation of this technique in the near field for tests in the wind tunnel takes into account the effects of convection and refraction and is discussed in [8].

Two types of analysis exist. The first is analog and is obtained in real time, from which it get its name, "Real Time Antenna".[1] It consists of summing the delayed signals of each of the microphones of the antenna, for a given focal point, and establishing the spectrum of the summed signal. The second is numerical and is obtained off-line, it gives an acoustic image that plots 100 spectra corresponding to 100 focal points (Figure 14).

Similarly, the programs to calculate the wave number spectra have been developed at ONERA. A completely similar analysis is given in reference [9].

[1] [Translators' note: Ther term "antenna" is meant in the sense of capable of being directive. In the United States, this would be called a beamformable or directional array.]

3. FLUCTUATING PRESSURE FIELD INDUCED BY A FULLY DEVELOPED TURBULENT BOUNDARY LAYER

Preliminary measurements have been made to characterize the fluctuating pressure field induced by a fully developed turbulent boundary layer at the velocity of 60 m/sec.

The results presented were obtained from signals furnished by the transducers comprising the longitudinal and transverse arrays.

The two types of analysis which have been used to characterize the fluctuating wall pressures are based one, on the longitudinal and transverse cross-spectral density functions (Corcos model [5]), and the other, on the wave number spectra.

3.1. Theoretical model, Corcos [5], and turbulence integral scales

The arrays of pressure transducers are found near the trailing edge, in a region of a weak positive pressure gradient. Under these conditions, the Corcos model [5], developed for a flat plate, remains valid. This has been verified experimentally by Schloemer [10].

The Corcos model describes a pressure field induced on a surface by a homogeneous turbulent boundary layer. The two dimensional field is expressed separately according to the longitudinal and transverse components:

(1) $$\Phi_{TBL}(\epsilon_1,\epsilon_3,\omega) = \Phi(\omega)\ A(\omega\epsilon_1/\overline{V})\ B(\omega\epsilon_3/\overline{V})\ \exp(-i\omega\epsilon_1/\overline{V})$$

where ϵ_1, ϵ_3 are the longitudinal and transverse separations for two points on the surface of the airfoil, $\overline{V}$ is the convection velocity, $\Phi(\omega)$ is the pressure spectral density and $A(\omega\epsilon_1/\overline{V})$ and $B(\omega\epsilon_3/\overline{V})$ are the longitudinal and transverse Corcos functions.

For the longitudinal and transverse directions, the turbulence integral scales are defined in the following way [11]:

(2) $$\ell_1 = \int_0^\infty A\left(\frac{\omega e_1}{\overline{V}}\right) e_1\, de_1 \Big/ \int_0^\infty A\left(\frac{\omega e_1}{\overline{V}}\right) de_1$$

and

(3) $$\ell_3 = \int_0^\infty B\left(\frac{\omega e_3}{\overline{V}}\right) e_3\, de_3 \Big/ \int_0^\infty B\left(\frac{\omega e_3}{\overline{V}}\right) de_3$$

With the functions $A(\omega\epsilon_1/\overline{V}) = \exp(-\eta_1\,\omega\epsilon_1/\overline{V})$ and $B(\omega\epsilon_3/\overline{V}) = \exp(-\eta_3\,\omega\epsilon_3/\overline{V})$ and a constant convection velocity $\overline{V}$, the previous equations are simplified [3,11] to give the following expressions:

(4) $$\ell_1 = \frac{\overline{V}}{\eta_1\omega} \quad ; \quad \ell_3 = \frac{\overline{V}}{\eta_3\omega}$$

where η_1 and η_3 are the decay factors of the functions $A(\omega\epsilon_1/\overline{V})$ and $B(\omega\epsilon_3/\overline{V})$.

3.2. Experimental results of the Corcos functions and the turbulence integral scales

The Corcos functions $A(\omega\epsilon_1/\overline{V})$ and $B(\omega\epsilon_3/\overline{V})$ correspond to cross-spectral functions of which the abscissa is put into a nondimensional form. They are derived from the classic coherence of the type $\gamma = G_{uv} / \sqrt{G_{uu}\, G_{vv}}$, where G_{uu} and G_{vv} are the autospectra of the signals u and v and G_{uv} is the cross-spectrum of these signals.

This definition, slightly different from that used by Corcos, nevertheless remains valid where the assumption of homogeneity is respected.

The coherences are calculated from signals furnished by the transducers located in proximity to the trailing edge.

For the longitudinal array, transducer number 16 has been chosen as the reference (Figure 3). Under these conditions, the separation distances between the transducers vary from 6 to 72 mm. Figure 4 represents the development of the longitudinal coherences, in the frequency band between 1 and 10 kHz.

The longitudinal coherences give rise to two remarks:

- the curves show a plateau at about 1 kHz, no matter what the gap between the transducers;

- beyond 1 kHz, the curves decrease rapidly.

For the transverse array, transducer number 7 has been chosen as the reference (Figure 3).

Although the transverse distances are shorter, 3 to 15 mm, the coherence functions are significant over a much more narrow frequency band compared to the longitudinal ones (Figure 5).

These transverse coherences are marked by a distinctly pronounced hump whose maximum is located near 1 kHz, no matter what the gap; beyond this value, these curves decrease rapidly.

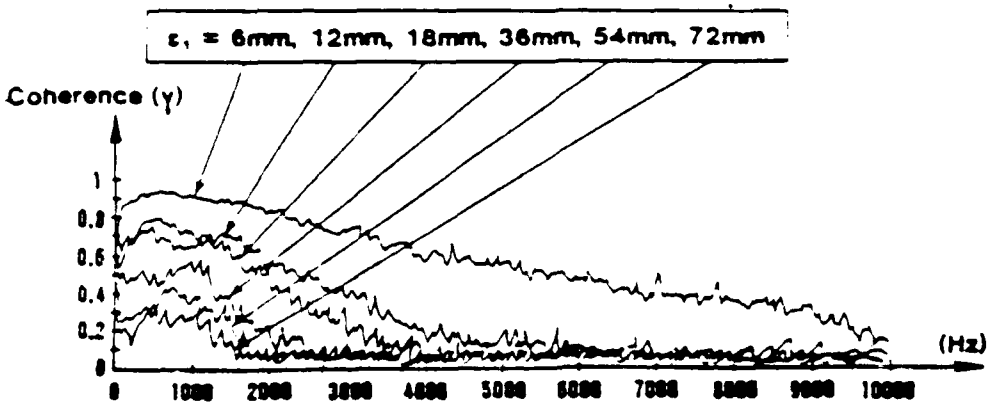

Figure 4. Longitudinal coherence functions analyzed up to 10 kHz, for different separations ϵ_1 - Transducer 16 as reference - U_o = 60 m/sec.

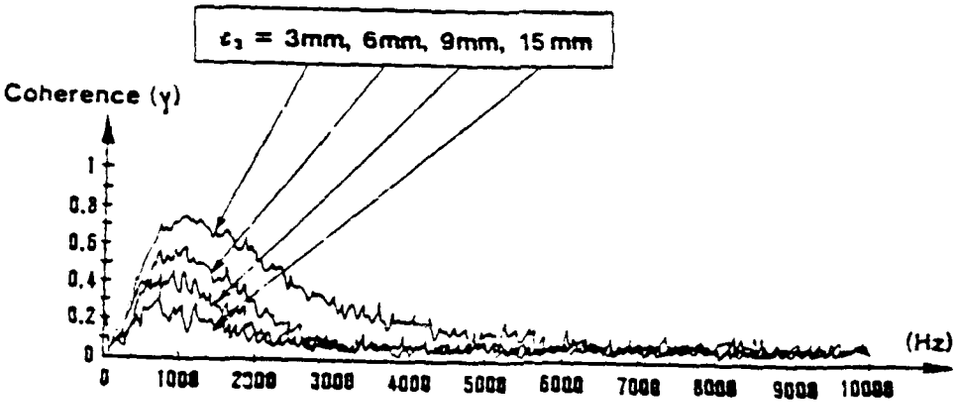

Figure 5. Transverse coherence functions analyzed up to 10 kHz, for different separations ϵ_3 - Transducer 7 as reference - U_o = 60 m/sec.

To transform the abscissas of these nondimensional curves, in the form $\omega\epsilon/\overline{V}$, requires the choice of a convection velocity $\overline{V}$. Figure 6 groups together the normalized cross-correlations between the signals coming from transducer 16, the reference, and the sensors which comprise the short and medium longitudinal arrays. The propagation times are then presented on Figure 7 as a function of longitudinal separations ϵ_1. The convection velocity is calculated from the slope of the curve (Figure 7) and is close to 0.7 U_o, when the separations ϵ_1, referenced to transducer 16, are less than 40 mm. A higher velocity, 0.8 U_o, is obtained for larger separations ϵ_1. This latter one has been kept to nondimensionalize the longitudinal and transverse coherence functions.

Figure 8 and 9 plot these results inferred from Figures 4 and 5 for different separations ϵ_1 and ϵ_3. From these sets of points it is clear the average curves $A(\omega\epsilon_1/\overline{V})$ and $B(\omega\epsilon_3/\overline{V})$ conform to the Corcos model. The function $B(\omega\epsilon_3/\overline{V})$ decreases much more rapidly than $A(\omega\epsilon_1/\overline{V})$. These functions are described analytically by decreasing exponentials of which the decay factors are equal to 0.17 and 0.9 respectively according to the longitudinal and transverse coordinates.

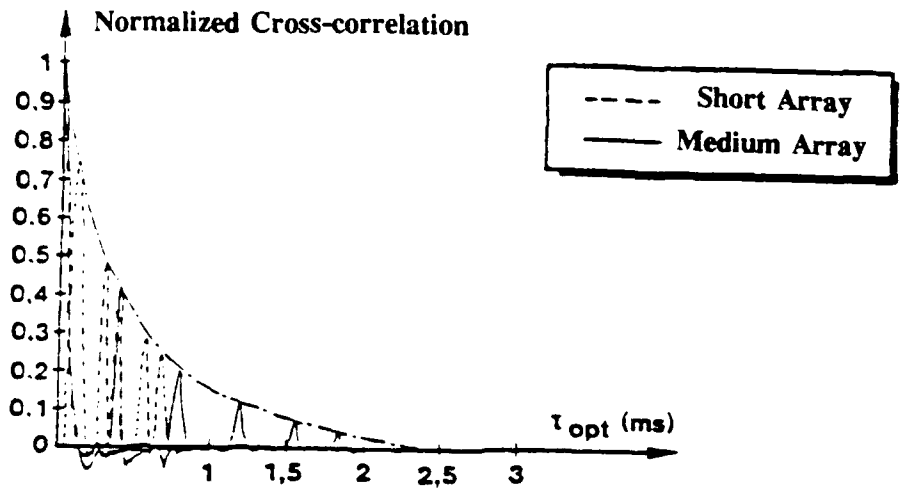

Figure 6. Normalized cross-correlations for different length longitudinal arrays of transducers - U_0 = 60 m/sec, ---- short array Δx_1 = 6 mm, —— medium Δx_1 = 18 mm

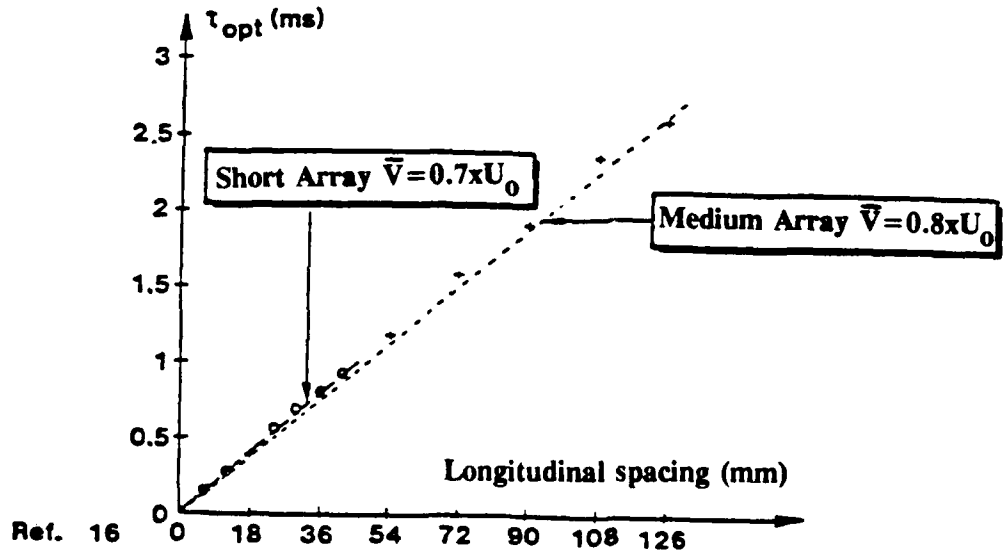

Figure 7. Variation of τ_{opt} as a function of longitudinal separations - U_0 = 60 m/sec, ---- short array Δx_1 = 6 mm, —— medium Δx_1 = 18 mm

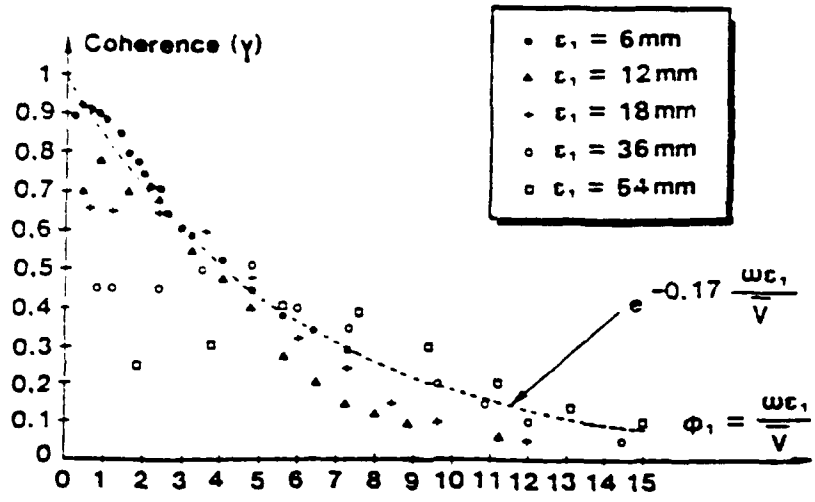

Figure 8. Longitudinal coherence as a function of a nondimensional number $\omega\epsilon_1/\bar{V}$. U_0 = 60 m/sec.

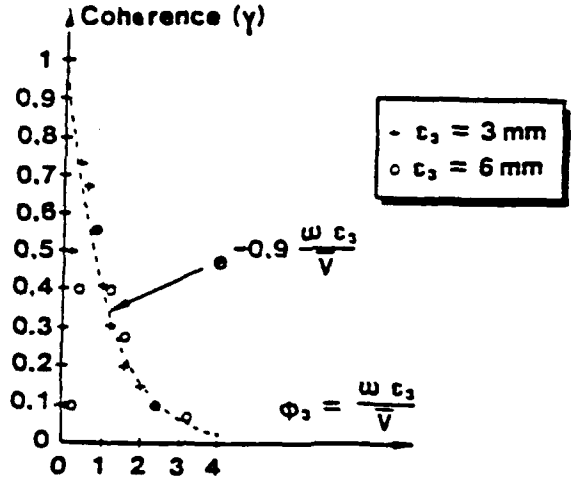

Figure 9. Transverse coherence as a function of a nondimensional number $\omega\epsilon_1/\bar{V}$. U_0 = 60 m/sec.

For a frequency of 1000 Hz, the turbulence integral scales, given by equation (4), give the following approximate values:

$$\ell_1 = \frac{0.8 \times 60}{2\pi \times 0.17 \times 10^3} = 45 \times 10^{-3} \text{ m} \quad (1.77 \text{ in.})$$

with $\eta_1 = 0.17$

and $$\ell_3 = \frac{0.8 \times 60}{2\pi \times 0.9 \times 10^3} = 8.5 \times 10^{-3} \text{ m} \quad (0.33 \text{ in.})$$

with $\eta_3 = 0.9$.

Table 1 shows similar results, obtained by Hogdson and Brooks [11], for a NACA 0012 airfoil with a chord of 60 cm. It is noted that the transverse decay factor η_3 of 0.9 as well as the convection velocity of 0.8 U_o are greater than those obtained by Hogdson.

3.3. Theory and definitions; wave number spectrum

The fluctuating pressure field induced by a fully turbulent boundary layer, has been described, until now, in terms of spatial cross-spectral functions according to the theory of Corcos.

Another way of modeling the homogeneous hydrodynamic pressure field is to consider it as a distribution of evanescent harmonic waves [3]. The pressure wave number spectrum is derived from the double space-time Fourier transform of the wall pressure $p(x_1,x_3,t)$, at the point x_1,x_3 taken on the surface of the airfoil.

(5) $$p(x_1,x_3,t) \xrightarrow{\text{F.T.}} P(k_1,k_3,\omega) \longrightarrow \Phi_{TBL}(k_1,k_3,\omega) = |P(k_1,k_3,\omega)|^2$$

In using the Corcos hypothesis, the expression for the wave number spectrum of the hydrodynamic pressure field simplifies:

(6) $$\Phi_{TBL}(k_1,k_3,\omega) = \Phi(\omega)\,\Phi(k_1)\,\Phi(k_3)$$

where the functions $\Phi(\omega)$, $\Phi(k_1)$ and $\Phi(k_3)$ are, respectively, the fluctuating pressure spectral density and the spatial Fourier transforms of the Corcos functions.

$$A\left(\frac{\omega|e_1|}{\bar{V}}\right) \exp\left(\frac{-i\omega e_1}{\bar{V}}\right) \quad , \quad B\left(\frac{\omega|e_3|}{\bar{V}}\right)$$

(7) $$\Phi_1(k_1) = \frac{1}{2\pi} \int_{-\infty}^{+\infty} A\left(\frac{\omega|e_1|}{\bar{V}}\right) \exp\left(\frac{-i\omega e_1}{\bar{V}}\right) \exp(-ik_1 e_1)\, de_1$$

with

$$A\left(\frac{\omega|e_1|}{\bar{V}}\right) = \exp\left(-\eta_1 \frac{\omega|e_1|}{\bar{V}}\right)$$

and

$$\Phi_3(k_3) = \frac{1}{2\pi} \int_{-\infty}^{+\infty} B\left(\frac{\omega |e_3|}{\bar{V}}\right) \exp(-ik_3 e_3)\, de_3 \tag{8}$$

with

$$B\left(\frac{\omega |e_3|}{\bar{V}}\right) = \exp\left(-\eta_3 \frac{\omega |e_3|}{\bar{V}}\right)$$

for a constant convection velocity V, the spectral functions $\Phi_1(k_1)$ and $\Phi_3(k_3)$ are simplified [3]:

$$\Phi_1(k_1) = \frac{\ell_1}{\pi}\left[\frac{1}{1 + \ell_1^2\left(\frac{\omega}{\bar{V}} - k_1\right)^2}\right] \tag{9}$$

and

$$\Phi_3(k_3) = \frac{\ell_3}{\pi}\left[\frac{1}{1 + \ell_3^2 k_3^2}\right] \tag{10}$$

3.4. Experimental results for wave number spectra $\Phi_1(\bar{k}_1,f)$, $\Phi_3(\bar{k}_3,f)$

The wave number spectra $\Phi_1(\bar{k}_1,f)$ and $\Phi_3(\bar{k}_3,f)$, presented in Figures 10 and 12, are obtained from the short longitudinal and short transverse arrays, for which equidistant distributions of Δx_1 and Δx_3 are 6 and 3 mm, respectively.

These results are presented in a three dimensional form with the amplitudes $\Phi_1(\bar{k}_1,f)$ and $\Phi_3(\bar{k}_1,f)$, expressed as a function of $\bar{k}_1$, $\bar{k}_3$, and f, where $\bar{k}_1$ and $\bar{k}_3$ are defined as being the ratio of a frequency over a velocity.

Figure 10 shows the appearance of spectral aliasing in k for frequencies above 2500 Hz. In this example, obtained with a spatial sample Δx_1 of 6 mm, the aliasing in k should be produced whenever $\bar{k} \geq \bar{k}_{max} = 1/2\ \Delta x_1 = 83\ m^{-1}$. This value is effectively reached by the components of the hydrodynamic pressure field, convected at the velocity of 0.7 U_o (Figure 11), when the frequencies are equal to or greater than 2500 Hz.

The energy of $\Phi_1(\bar{k}_1,f)$ is concentrated in the convective region in which the trace in the plane $(\bar{k}_1,f)$, at the mean of the grey shaded representation, gives approximately a straight line (Figure 11).

The convective velocity, derived from the slope of this straight line, is equal to 0.7 U_o. A similar result for $\Phi_1(\bar{k}_1,f)$ has been investigated from the medium longitudinal array, where the separation Δx_1 between the transducers is equal to 18 mm. The preceding remarks remain true, but the velocities obtained are equal to 0.8 U_o. These observations parallel the conclusions drawn from Figure 7.

It follows then that the medium and small scale turbulent boundary layer structures are spatially filtered

by the longer arrays and that their convection velocity 0.7 U_o is less than those of structures of much larger dimensions which stabilize, from the array being longer, in the vicinity of 0.8 U_o.

Distance between sensors: 6.0 mm
500 Averages
Point Number: 22
Number of sensors: 10
U_o: 60.0 m/sec

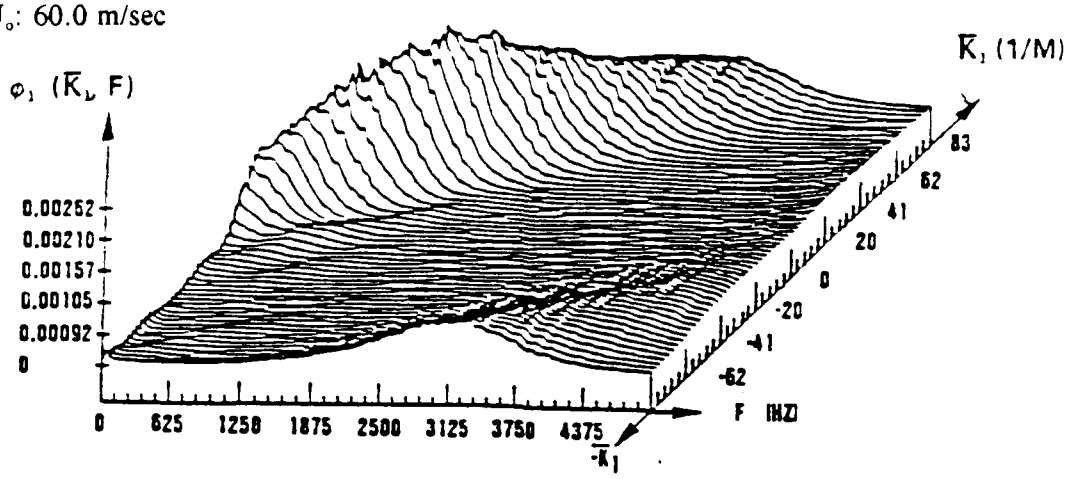

Wave Number Spectrum Φ_1 ($\bar{K}_1$,F)

Figure 10. Wave number spectrum $\Phi_1(k_1,f)$ obtained from the short longitudinal array. U_o = 60 m/sec.

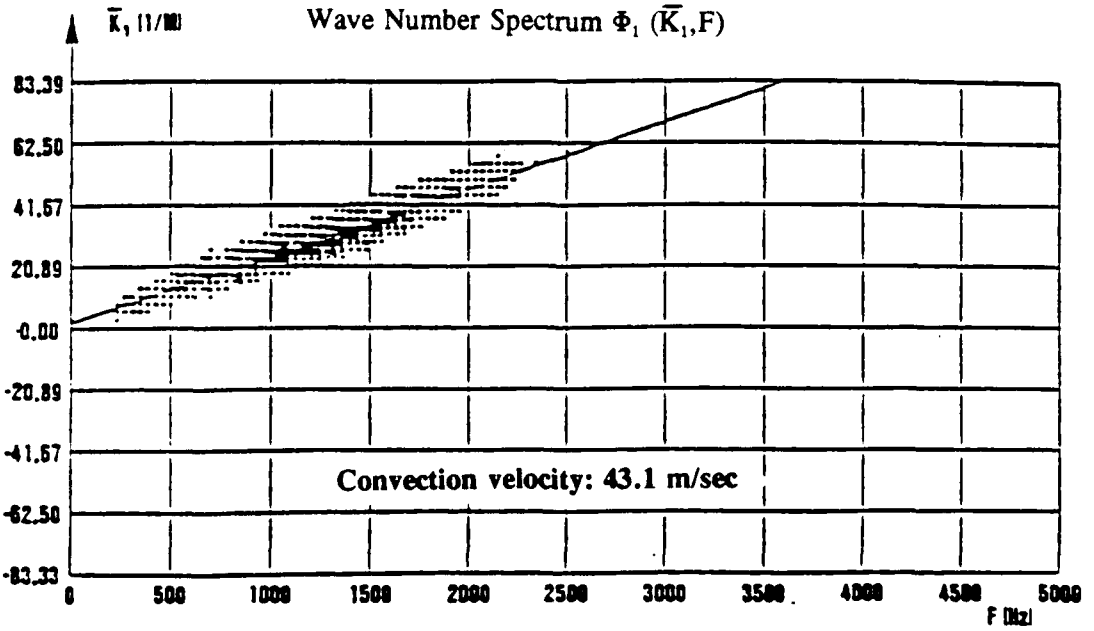

Figure 11. Projection of the wave number spectrum $\Phi_1(\bar{k}_1,f)$ on the $(\bar{k}_1,f)$ plane.

These experimental values of convection velocity remain greater than those of Hodgson (see Table 1).

Table 1.

Study	η_1 (m)	η_3 (m)	V	CONDITIONS
Garcia - Gerard	+0.17	+0.9	$\simeq 0.8\ U_o$	12% NACA Profile Chord 50 cm U_o = 69 m/sec
Hogdson - Brooks	+0.14	+0.58	$\simeq 0.8\ U_o$	12% NACA Profile Chord 60 cm U_o = 69 m/sec
Corcos	+0.11	+0.71		Flat plate U_o = 69 m/sec

The wave number spectrum $\Phi_3(k_3,f)$, obtained from the transverse array, is symmetrical in relation to the plane $k_3 = 0$ and centered around the frequency of 1 kHz (Figure 12).

Distance between sensors: 3.0 mm
500 Averages
Point Number: 22
Number of sensors: 9
U_o: 60.0 m/sec

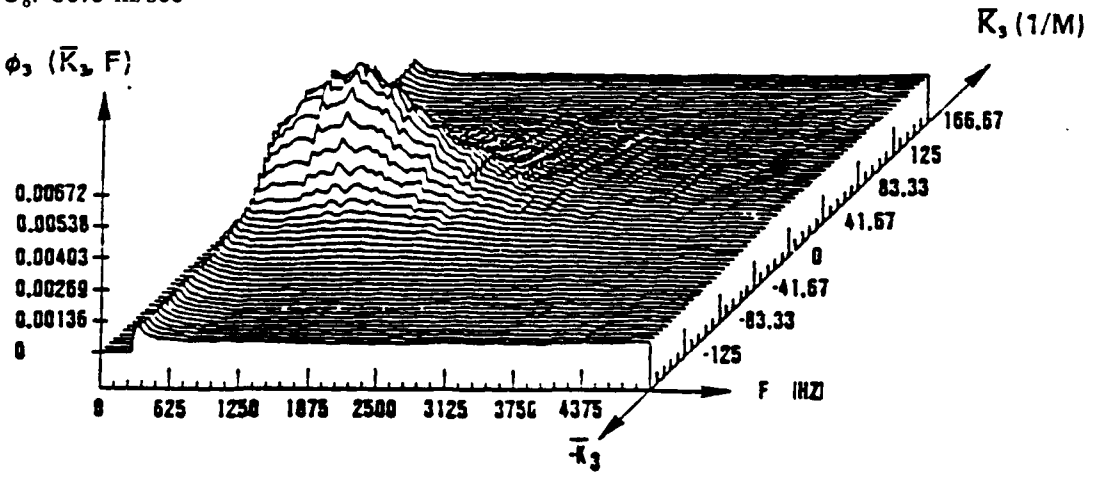

Wave Number Spectrum Φ_3 ($\bar{K}_3$,F)

Figure 12. Wave number spectrum $\Phi_3(\bar{k}_3,f)$ obtained from the short transverse array. U_o = 60 m/sec.

4. RADIATED NOISE

The prediction calculation, based on the theory of Howe [4], is given in the beginning of this paragraph.

The noise radiated by the airfoil is localized and identified by acoustic imagery techniques and from analysis of cross spectra. The measurement of this noise, due to the interaction of the stable flow with the airfoil, is obtained beginning with the autospectra of signals furnished by two microphones, placed symmetrically. A comparison between the measured and calculated radiated noise from a simplified formulation, concludes this chapter.

4.1. Calculated predictions based on the theory of Howe

Howe [4] proposes an extension of Lighthill's analogy to a stationary, irrotational, non-viscous, non-conducting, and isentropic mean flow. The solving of the wave equation for enthalpy allows one to express:

- the "hydrodynamic" pressure induced by the turbulent boundary layer, in the neighborhood of the trailing edge; and

- the radiated acoustic pressure in the far field.

Howe obtained a relation between the radiated noise spectrum and the wave number spectrum $\Phi_{TE}(k_1, \omega \cos\alpha/V, \omega)$ of the hydrodynamic pressure that, in the far field, is written:

$$S(\omega) = \frac{2\left(\frac{\overline{V}}{c}\right) L \sin^2\left(\frac{\theta}{2}\right)}{\pi R^2 \left[1 - \frac{\overline{V}}{c}\right]} \int \Phi_{T.E.}\left(k_1, \frac{\omega \cos\alpha}{c}, \omega\right) dk_1 \tag{11}$$

where V equaling 0.8 U_o, is the convection velocity, L, the span, R, the distance from the trailing edge to the receiver, and θ, the angle of observation.

For an observation angle of $\theta = 90^\circ$, the preceding equation reduces, according to Brooks and Hodgson [11], to.

$$S(\omega) \frac{1}{\sqrt{2}\,\pi^2 R^2} \left(\frac{\overline{V}L}{c}\right) \frac{\ell_3 \Phi(\omega)}{\left(1 - \frac{\overline{V}}{c}\right)} \tag{12}$$

with $\int \Phi_{TE}(k_1,0,\omega)\, dk_1 = \ell_3(\omega)\, \Phi(\omega)$.

4.2. Radiated Noise Measurement

4.2.1. Analysis of radiated noise using microphone 63 and acoustic imagery.

The first estimate of radiated noise by the airfoil is obtained by direct comparison of the spectra of the acoustic pressure emitted by the airfoil to those of the background noise of the wind tunnel.

Figure 13 presents the spectral analyses made in the frequency band 300 Hz - 5 kHz, from signals furnished by microphone 63. The following points are emphasized:

- the emission frequency band for the airfoil is located, in this first approach, in a few hundred hertz around 2 kHz; and

- comparative study of the spectra (Figure 13) makes apparent two very distinct regions: one corresponds to spreads greater than 10 dB, high pass filtered at 300 Hz, in the frequency band less than 1 kHz, the other to spreads greater than 5 dB for medium and high frequencies.

Figure 14 represents an acoustic image composed of 100 focal points distributed symmetrically along the length of the trailing edge over a distance of $\pm$ 2.50 m. When the airfoil is present in the test flow, two sources stand out distinctly. The acoustic imagery sections (Figure 15), for frequencies from 850 to 1000 Hz, localize a source at 1.15 m and the other at-0.68 m.

In effect, the airfoil with a 3 m span interacts with a jet, shown schematically on Figure 2, composed of a potential cone and a mixing zone. These two types of flow, one laminar and one turbulent, give birth to two sources, a low frequency one in the mixing zone, the other one at medium and high frequencies in the potential cone.

The two parasitic sources localized by the acoustic imagery technique (Figure 14) result from the interaction of the mixing zone with the airfoil.

4.2.2. Localization and identification of the acoustic source, coming from interaction with the potential cone

The localization and the identification of the sought after aerodynamic source has been established from cross-spectral analysis between pressure transducers near the trailing edge and a "far field" receiver.

In order to partly separate itself from these two interfering sources, the "real time" acoustic antenna has been focused, using analog methods, on the instrumented part of the airfoil.

The normalized cross-correlation function (Figure 16) between the analog signals furnished by the "real time" antenna and pressure transducer 7, analyzed from 500 Hz to 2 kHz, shows a delay of 14.5 ms, which effectively corresponds to the time taken by the sound pressure to propagate from a region situated near the trailing edge towards the antenna.

We emphasize that, for the relative positions of the source and the receiver in relation to the mixing zone of the jet, the combined influence of the effects of convection and refraction on the propagation is negligible [12].

The corresponding cross-spectrum (Figure 17) analyzed in a frequency band of 500 Hz - 4 kHz, gives a phase plot which, although noisy, settles at a value of $-\pi/4$ [2] in the 500 Hz to 2 kHz range. This value of the phase is obtained after having taken into account the correction for the electronic phase differences

[2] [Translators' note: The phase plot provided in Figure 17 actually shows this as $+3\pi/4$. So there must have been a $-\pi$ electronic phase correction.]

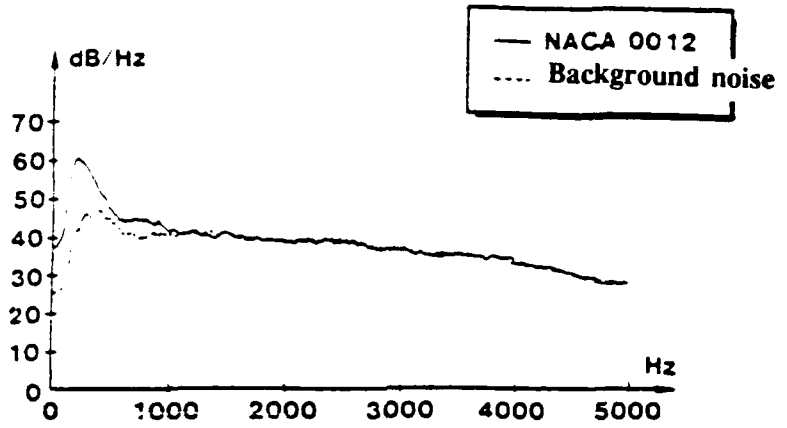

Figure 13. Comparison of radiated spectra with and without airfoil in the flow. Microphone 63. U_0 = 60 m/sec.

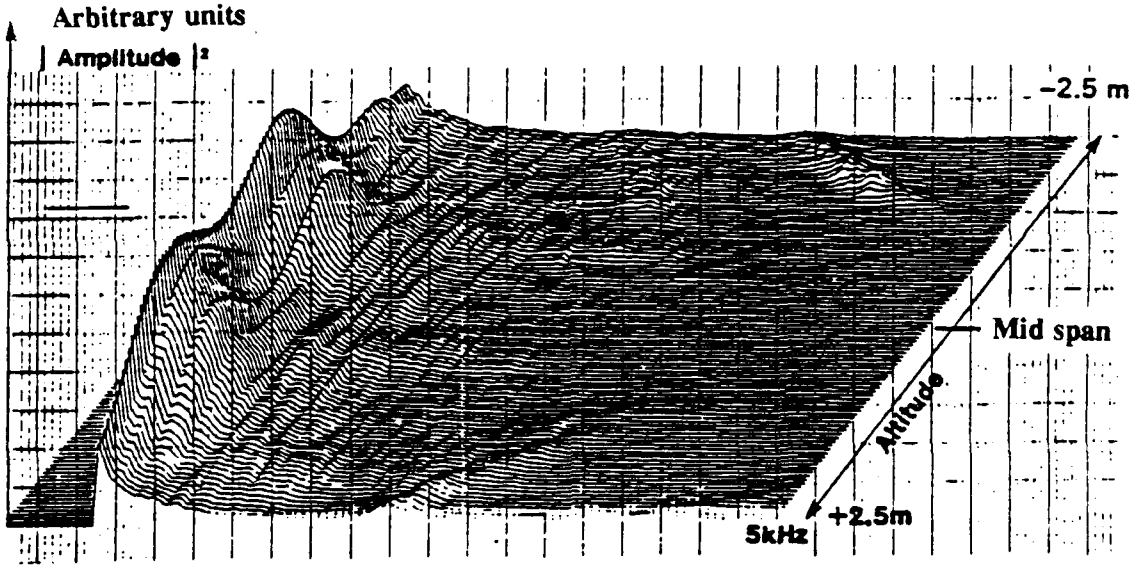

Figure 14. Spanwise "acoustic image" of the NACA 0012 airfoil, U_0 = 60 m/sec.

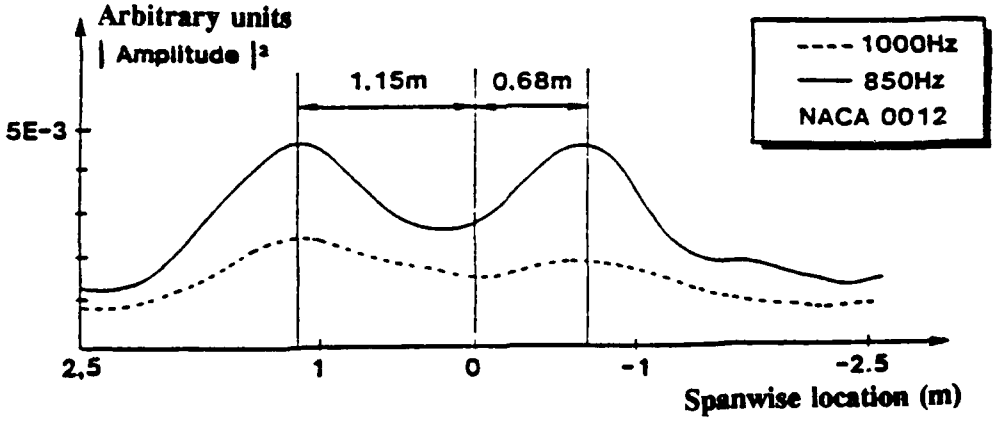

Figure 15. Sections obtained from the acoustic image for frequencies of 850 and 1000 Hz.

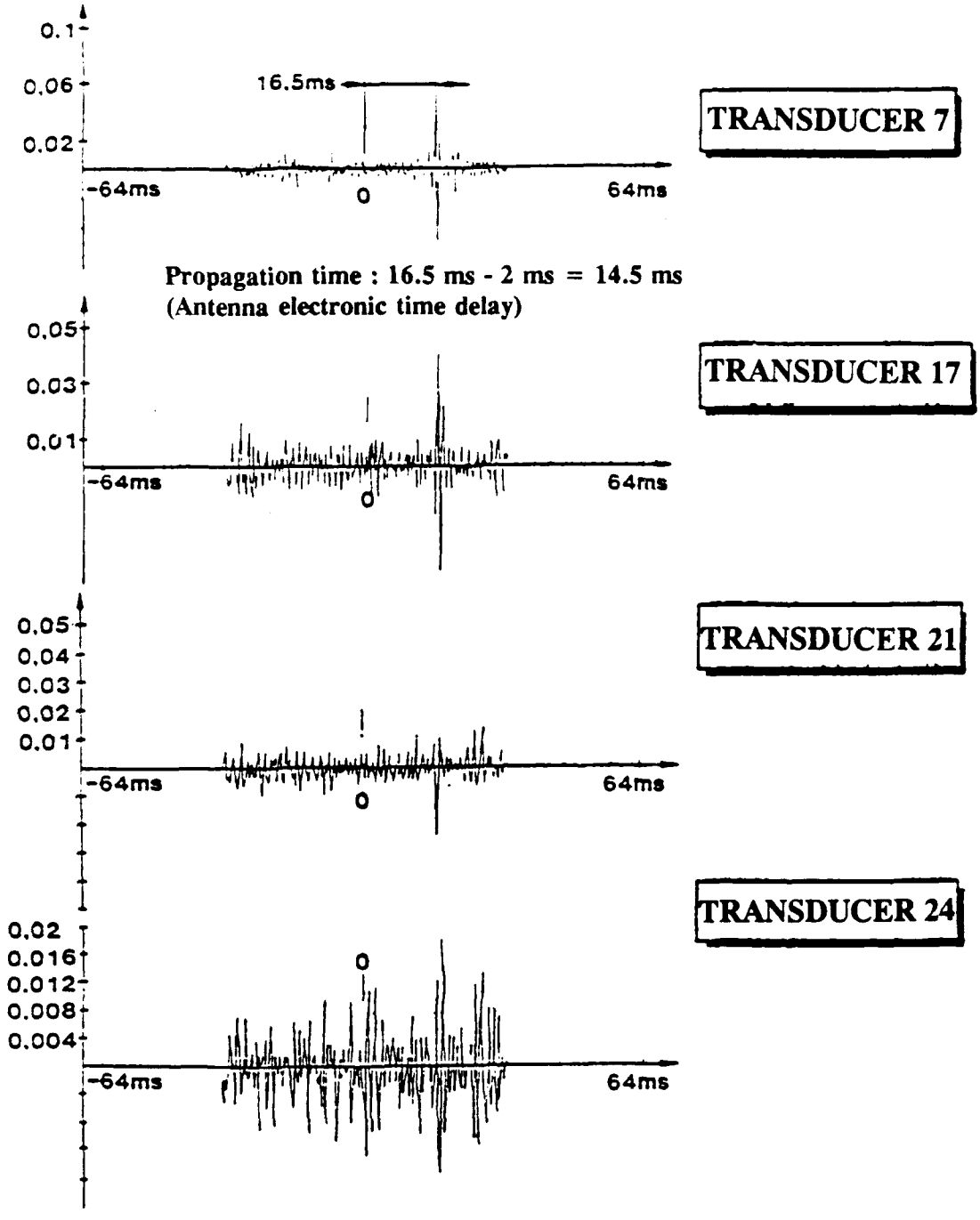

Figure 16. Cross-correlation functions between the acoustic antenna (real-time) and the flush mounted pressure transducers indicated.

a) transducer 7
b) transducer 17
c) transducer 21
d) transducer 24

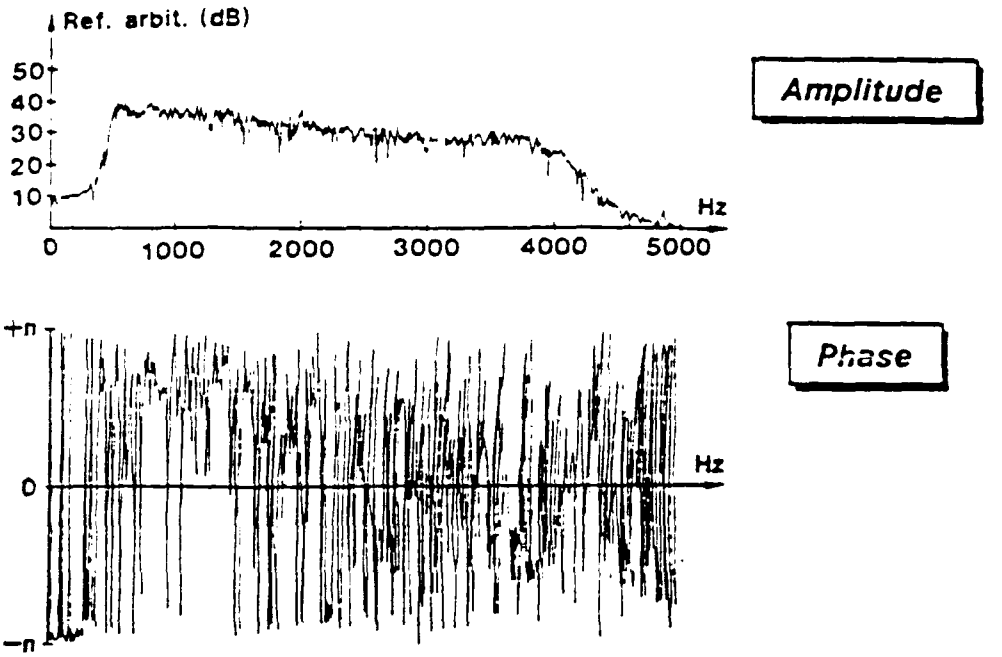

Figure 17. Cross-spectrum between the acoustic antenna (real-time) and flush mounted pressure transducer number 7. Frequency range of analysis 500 Hz - 4 kHz, U_0 = 60 m/sec.

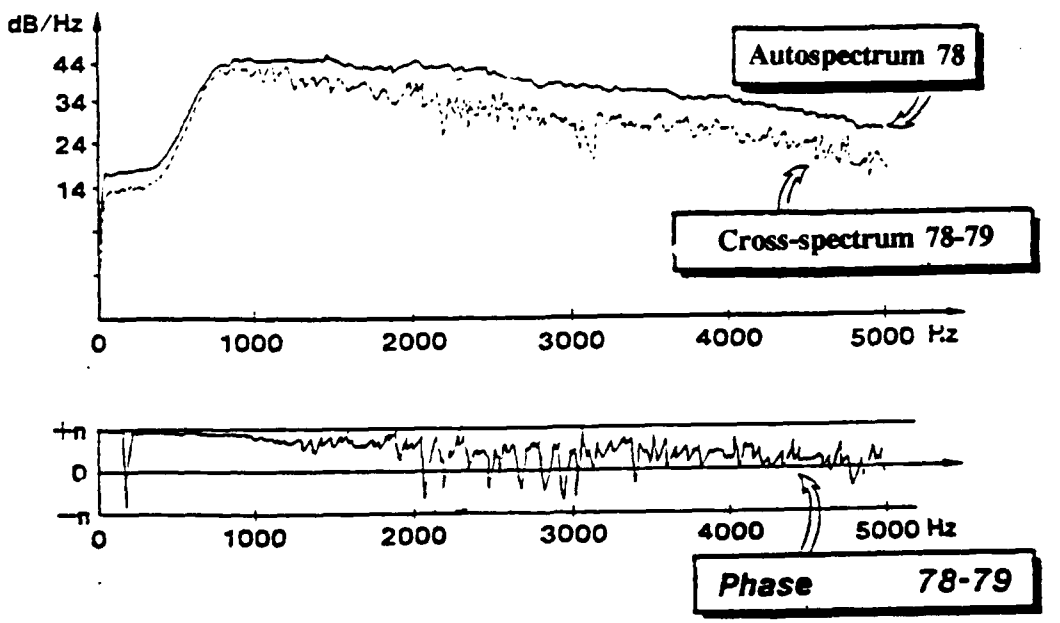

Figure 18. Cross-spectrum and autospectrum from microphones 78 and 79, U_0 = 60 m/sec.

of the Entran transducers with the B&K microphones. Moreover, the correlation between the signals, furnished by transducers 17, 21, 24 (Figure 3) and the antenna becomes even weaker since the transducer considered is displaced from the trailing edge (Figure 16).

These results permit us to state that:

- the source is localized in the region of the trailing edge; and
- the sought after acoustic source emits in a frequency band of about 500 Hz - 2 kHz

4.2.3. Measure of radiated noise using two microphones 78 and 79 symmetric about the airfoil

The techniques put in place previously have allowed the localization and identification of radiated noise by the trailing edge of the airfoil situated in the steady part of the flow. On the other hand, they do not allow us, currently, to recover the radiated noise spectrum.

For that, we have taken the approach of Brooks and Hogdson [11] that consists of extracting, from the background noise of the wind tunnel, the noise emitted by the airfoil by using the cross-spectrum obtained from the signals furnished by the microphones placed symmetrically apart and from others on the model.

The results, presented in Figure 18, are obtained for microphones 78 and 79 (Figure 2). The spectral analysis has been high pass filtered above the frequency of 800 Hz in order to distinguish it from the parasitic low frequency.

The plotted curves, in Figure 18, confirm the selective character, in the high frequencies, of the cross-spectrum from the signals furnished by microphones 78 and 79, compared to the radiated noise spectrum. The phase of the cross-spectrum is very well defined and shows an opposition, in the frequency band of 4.5 kHz that characterizes the dipole nature of the studied source.

The slope of these phases is probably due to a very slight variation between the propagation times, on the order of 0.1 ms, of the acoustic pressure that reaches microphones 78-79, for which the positions are not perfectly symmetric.

Another experimental result of measured noise is presented in Figure 19 for a velocity of 70 m/sec, but with the span and the distance from the trailing edge to the receiver reduced, allowing a comparison with the measurements of Brooks and Hogdson [11].

The reduction factor depends only on the geometry of the airfoil, the spectral densities $\Phi(\omega)$, and the turbulence integral scales ℓ_3 being considered fixed. The factor is deduced from the simplified formula [12] of Howe and is equal to $10 \log (L_H/L) + 10 \log (R/R_H)^2$, where L_H and R_H are, respectively, the span length and distance from the trailing edge to the receiver for the Hogdson model and L and R correspond to those of this study.

Only the chord length, 60 cm for Hogdson and 50 cm for this study, differ. A comparison of this measurement reduced from radiated noise with that of Hogdson, for a NACA 0012 airfoil of span 40 cm and a distance of 1.2 m from the trailing edge to the receiver and for a velocity of 70 m/sec, results in a overlaying of the curves (Figure 19).

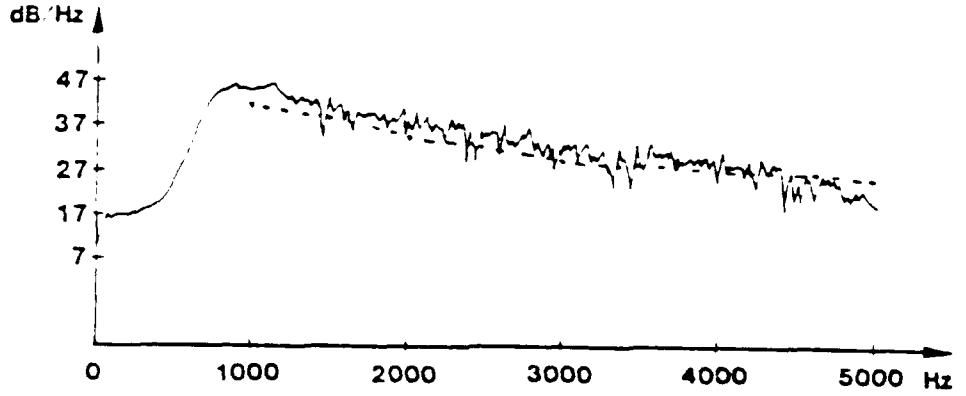

Figure 19. Comparison with the radiated noise measurement obtained by Brooks and Hogdson (---). U_0 = 70 m/sec.

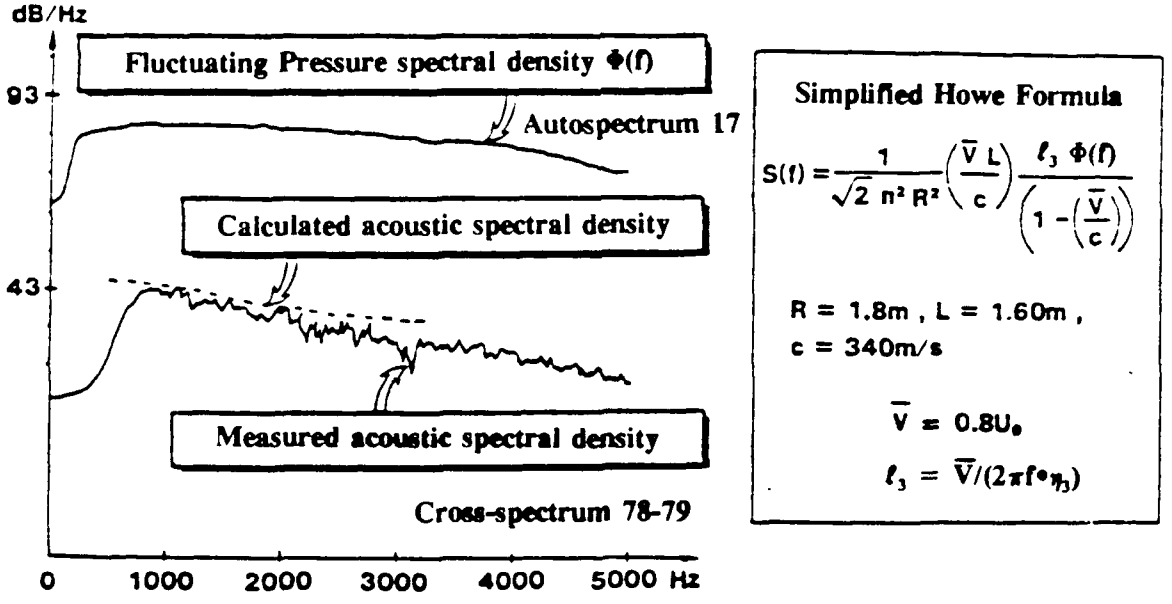

Figure 20. Comparison of measured and calculated radiated noise. NACA 0012 airfoil. U_0 = 60 m/sec.

4.3. Overlaying of calculated and measured radiated noise for a NACA 0012 profile in a uniform flow

The prediction calculation, based on the simplified formulation [12] of Howe, is applied to the radiated noise by the NACA 0012 airfoil, for the flow speed U_o = 60 m/sec. The calculations require, in addition to the geometry of the airfoil - receiver group, two other input data:

- the spectral density of the fluctuating pressure near the trailing edge $\Phi(\omega)$ (the spectral density of transducer 17 is represented in Figure 20); and

- the transverse turbulence integral scale of ℓ_3, deduced from measurements of the wall pressure (paragraph 3.2.).

Only the interaction between the potential cone and the airfoil is taken into account. Consequently, the sought after source is distributed along the length of the span submitted to a steady flow, that is about 1.6 m.

In Figure 20, the prediction calculation is compared to the measured radiated noise by the airfoil, obtained previously from the cross-spectrum between the two microphones 78 and 79; the difference is of the order of a few decibels in the frequency band 800 Hz - 3 kHz.

This technique has been used by Hogdson [11]. The difference between the experimental results and the calculated results is analogous to the one presented in Figure 20.

5. CONCLUSIONS

Acoustical imaging and cross-spectral techniques allow, on the one hand, the highlighting of an acoustic source in the vicinity of the trailing edge and, on the other hand, identifying the range of frequencies of emission of this source (500 Hz - 2 kHz).

The two microphones 78 and 79, symmetrically placed in relation to the airfoil, allow the establishment of the dipole nature of the studied source, as well as its measurement.

A comparison of the measured results with those obtained by Brooks and Hogdson, under similar velocity conditions, similar span, and trailing edge to receiver distance, is entirely satisfactory.

The estimation of noise radiated by the trailing edge from the theory of Howe, requires, in addition to the airfoil-receiver geometry, knowledge of the wall pressure field, induced by the fully developed turbulent boundary layer established in the region of the trailing edge.

Two techniques are used in order to model this boundary layer:

- the wave number spectrum of the fluctuating pressure, $\Phi_{TE}(k_1, k_3, \omega)$; and

- the pressure spectral density $\Phi(\omega)$ and the turbulence integral scales, ℓ_1 and ℓ_3, according to the model of Corcos.

The input data $\Phi(\omega)$ and ℓ_3, deduced from wall pressure measurements, are introduced in the simplified expression by Howe in order to estimate the radiated noise in the far field, at the angle $\theta=90^{\circ}$. The measurement and the estimation of radiated noise by the trailing edge of an airfoil agrees, within a few decibels, in the frequency range of 800 Hz - 3 kHz, for a velocity of 60 m/sec.

Our subsequent objectives are to use the more general estimation from Howe who introduced a model of the turbulent boundary layer in the form of a wave number spectrum. The predicted noise levels will be verified by other flow conditions at the trailing edge, obtained by varying the airfoil leading edge.

REFERENCES

[1] Ffowcs Williams, J. E. and Hall, L. H., 1970, "Aerodynamic sound generation by turbulent flow in the vicinity of a scattering half-plane", *J. Fluid Mech.* **40**, pp. 657-670.

[2] Chase, D. M., 1972, "Sound radiated by turbulent flow off a rigid half-plane as obtained from a wave vector spectrum of hydrodynamic pressure", *J. Acous. Soc. Am.* **52**, pp. 1011-1023.

[3] Chandiramani, 1974, "Diffraction of evanescent waves with application to aerodynamically scattered sound and radiation from an unbaffled plate", *J. Acous. Soc. Am.* **56(1)**.

[4] Howe, M. S., 1977, "A review of the theory of trailing edge noise", Bolt Beranek and Newman Report No. 3679, December 1977.

[5] Corcos, G. N., 1964, "The structure of the turbulent pressure field in boundary layer flows", *J. Fluid Mech.* **18**, pp. 353-378.

[6] Pauzin, S. and Biron, D., "Caractérisation en pression de capteurs miniatures ENTRAN", Report No. 2/2184.00, (CERT).

[7] Gilchrist, R. B. and Strawderman, W. A., 1965, "Experimental hydrophone size correction factor for boundary layer pressure fluctuations", *J. Acous. Soc. Am.* **38**, pp. 298-302.

[8] Elias, G. and Malarmey, C., 1983, "Utilisation d'antennes focalisées pour la localisation des sources acoustiques", llème Congrès Int. d'Acoustique, Paris, 19-27 July 1983, ONERA TP No. 1983-75.

[9] King, L. A., 1983, "Wavenumber frequency analysis of the self-noise of a structure moving through water", AIAA paper 83-0686.

[10] Schloemer, H. H., 1967, "Effects of pressure gradients on turbulent boundary layer wall pressure fluctuations", *J. Acous. Soc. Am.* **42**, pp. 93-113.

[11] Hogdson, T. H. and Brooks, T. F., 1980, "Prediction and comparison of trailing edge noise using measured surface pressures", AIAA paper 80-0977.

[12] Candel, S. M., 1978, "Etudes théoriques et experimentales de la propagation acoustic en milieu inhomogene et en mouvement", These Universite Paris VI, ONERA Technical Note No. 1978-1.